Evaluation of ISLSCP Initiative II FASIR and GIMMS NDVI products and implications for carbon cycle science

Forrest Hall,[1,2] Jeffrey G. Masek,[1] and G. James Collatz[1]

Received 25 April 2006; revised 15 August 2006; accepted 9 October 2006; published 23 November 2006.

[1] Integration of NDVI data into ecological and biogeochemical modeling has placed more stringent requirements on the accuracy and stability of the measurement. We compare two recent AVHRR NDVI data sets included as part of ISLSCP Initiative II: (1) the Fourier-Adjusted, Sensor and Solar zenith angle corrected, Interpolated, Reconstructed (FASIR) monthly time series and (2) the Global Inventory Modeling and Mapping Studies (GIMMS) monthly time series. Although both started with nearly identical composited AVHRR GAC data sets, each data set has been processed differently to reduce sensor, atmospheric, and illumination effects that vary over time. We find that the resulting absolute NDVI data records differ substantially and consistently for large parts of the globe. These differences also propagate into the NDVI anomaly record (e.g., deviations from monthly or annual means) particularly in the 1984–1985, 1994 periods. To assess the effect of these differences on predictions of land surface CO_2 fluxes, the fraction of absorbed photosynthetically active radiation (fPAR) was calculated from each record, and used to drive a biogeochemical model (CASA). On a global basis, calculated net ecosystem exchange shows large variability inherited from the NDVI records. However, these variations do not match global CO_2 fluxes derived from atmospheric inversion of CO_2 concentration measurements. We conclude that other processes (burning, physiologic response to stress) are likely responsible for major anomalies in the observed global land net carbon fluxes to the atmosphere during the period 1982–1998.

Citation: Hall, F., J. G. Masek, and G. J. Collatz (2006), Evaluation of ISLSCP Initiative II FASIR and GIMMS NDVI products and implications for carbon cycle science, *J. Geophys. Res.*, *111*, D22S08, doi:10.1029/2006JD007438.

1. Introduction

[2] A primary accomplishment of land remote sensing over the last thirty years has been the development of global vegetation indices for monitoring the terrestrial environment. The contrast between near-infrared and visible reflectance for characterizing vegetation ''greenness'' was originally recognized using field radiometers [*Birth and McVey*, 1968] and early Landsat imagery [*Rouse et al.*, 1974]. Gradually, the Normalized Difference Vegetation Index (NDVI) became the standard formulation, in large part because of its insensitivity to variability in illumination conditions [*Tucker*, 1979]. NDVI is formally defined as $(\rho_{nir} - \rho_{vis})/(\rho_{nir} + \rho_{vis})$ where ρ_{nir} is either the surface or top of atmosphere reflectance in the near-infrared wavelength range and ρ_{vis} is for the visible wavelength range. For narrowband sensors, reflectance in the red wavelength is usually substituted for ρ_{vis}.

[3] Increased concern with global climate and environmental changes in the 1980s, coupled with the cost of Landsat data as a result of privatization of the Landsat program, spurred researchers to use data from the NOAA Advanced Very High Resolution Radiometer (AVHRR) instruments. Although these instruments were designed for operational meteorology, their capacity to acquire daily, global data in visible and near-infrared wavelengths made them useful for tracking vegetation conditions. NOAA began producing the first vegetation index products from AVHRR in 1982 (the Global Vegetation Index or GVI product). Early analyses of the GVI products focused on basic biogeography, seasonality of vegetation patterns at continental scales, and correlations with atmospheric carbon dioxide measurements [*Justice et al.*, 1985; *Goward et al.*, 1985; *Tucker et al.*, 1985, 1986]. Although critical for establishing the utility of global satellite observations for monitoring vegetation, these early studies primarily focused on qualitative relations between the NDVI and vegetation properties. Gradually, researchers developed quantitative relations between NDVI and biophysical variables controlling vegetation productivity and land/atmosphere fluxes [*Asrar et al.*, 1984; *Sellers*, 1985; *Nemani and Running*, 1989]. Principal among these are leaf area index (LAI) and the fraction of absorbed photosynthetically active radiation (fPAR). *Hall et al.* [1992] found that NDVI responded almost linearly to the fraction of incident photosynthetically active radiation absorbed by the photosynthetically active

[1]NASA Goddard Space Flight Center, Greenbelt, Maryland, USA.
[2]Also at Joint Center for Earth Systems Technology, University of Maryland Baltimore County, Baltimore, Maryland, USA.

0148-0227/06/2006JD007438

tissue in the canopy (fPAR) and was insensitive to that absorbed by nonphotosynthetic tissue.

[4] These pioneering studies led to a current generation of ecosystem models that use satellite-based vegetation indices for predicting carbon, energy, and water fluxes in response to climate variability and ecosystem disturbance [e.g., *Randerson et al.*, 1996; *Sellers et al.*, 1996; *Kaminski et al.*, 2002; *van der Werf et al.*, 2004]. Ideally, these models should provide understanding of how trends in climate since the early 1980s have affected vegetation patterns, and how these feed back to the climate system [e.g., *Nemani et al.*, 2001; *Bounoua et al.*, 2000]. Several carbon and climate studies have shown that prescribing seasonal phenology of vegetation using NDVI based products produces more realistic model simulations than a phenology based on climatology [*Kang et al.*, 2006]. NDVI products are also used to validate phenology and interannual variability in vegetation grown in so-called dynamic vegetation models [*Dickinson et al.*, 1998; *Zeng et al.*, 1999; *Lucht et al.*, 2002].

[5] The integration of NDVI observations into physical models placed more stringent requirements on the accuracy and stability of the measurement. From the perspective of long-term ecosystem monitoring, the AVHRR observation record suffers from numerous deficiencies including poor sensor calibration, poor intercalibration between successive NOAA platforms, wide variations in solar-view geometry, atmospheric contamination, cloud contamination, and the systematic drift in acquisition time during the life of individual missions [*Gutman*, 1991; *Goward et al.*, 1993; *Los et al.*, 1994; *Privette et al.*, 1995; *Gutman*, 1999]. As a result, the AVHRR Global Area Coverage (GAC) record has been reprocessed several times since the mid-1990s in an effort to mitigate these deficiencies [*Townshend*, 1994; *Tucker et al.*, 1994; *James and Kalluri*, 1994; *Goward et al.*, 1994; *Los et al.*, 2000; *Tucker et al.*, 2005].

[6] Because NDVI is a ratio of differences between two adjacent bands, it is largely *insensitive* to variations in illumination intensity. However, NDVI is sensitive to sensor, atmospheric and illumination effects that differ between bands. Band calibrations, for example, have changed frequently between the five NOAA AVHRR instruments that acquired the 22-year NDVI record for Initiative II. In addition, natural variability in atmospheric aerosols and column water vapor have created surface-independent variations in the NDVI record. Finally, over the period of record there were two major volcanic eruptions, El Chichon in 1982 and Mt. Pinatubo in 1991 [*Rosen et al.*, 1994] that injected large quantities of aerosols into the Earth's stratosphere. These aerosols, along with smoke from biomass burning and dust from soil erosion and other factors, introduce significant variability in the AVHRR NDVI record. These constituents have significantly different effects on AVHRR channel 1 (visible) and channel 2 (near infrared). Variations in the illumination conditions over the period of record also introduce spurious variation into the NDVI signal. The AVHRR sensors flew aboard the afternoon NOAA platforms, beginning with the NOAA 7 satellite launched in January of 1980, continuing on NOAA 9, 11 and 14. The NOAA satellite overpass times drifted from the nominal 1:30 pm overpass time by as much as 4 1/2 hours toward evening, creating variable illumination and view angles (see Figure 1).

[7] The ISLSCP Initiative II data collection contains two AVHRR NDVI time series, processed using two different algorithms, both aimed at reducing the above mentioned effects on the NDVI signal. These are (1) The Fourier-Adjusted, Sensor and Solar zenith angle corrected, Interpolated, Reconstructed (FASIR) monthly time series 1981–1998 [*Los et al.*, 2005; *Hall et al.*, 2006] and (2) The Global Inventory Modeling and Mapping Studies (GIMMS) monthly time series, 1981 to 2000 [*Tucker et al.*, 2005]. The inclusion of these data sets provides the land science community with a consistently gridded, set of vegetation records for driving process models. Although both data sets start with the NOAA AVHRR 4 km resolution GAC data, each has chosen unique processing approaches for producing a consistent NDVI record. Both the GIMMS and FASIR records were originally produced at 8 km resolution, but are represented within the International Satellite Land Surface Climatology Project (ISLSCP) Initiative II collection using the standard 0.25, 0.50, and 1.0 degree resolution latitude-longitude grids. The ISLSCP Initiative II minimum 0.25 degree equal-angle grid, a fourfold increase in spatial resolution over the Initiative I collection, was chosen to correspond to data input requirements for carbon, water and energy models.

[8] This paper presents a comparison between the ISLSCP FASIR and GIMMS NDVI data sets, with a specific focus on the applicability of the ISCLSCP data sets to carbon cycle modeling. We first explore differences between the data sets in terms of absolute NDVI, including comparisons with Landsat-derived NDVI from single clear-sky observations. We then examine differences in terms of interannual anomalies. Finally, we address the implications of observed NDVI variability for global carbon cycle modeling.

2. Description of ISLSCP NDVI Data Sets

[9] Key aspects of the FASIR and GIMMS algorithms and their differences are highlighted below in Table 1. The AVHRR raw data used for GIMMS and FASIR are somewhat different. Both used maximum NDVI composited data to reduce atmospheric and cloud contamination. However, FASIR used the cloud-screened Pathfinder AVHRR bands 1 and 2 series of *James and Kalluri* [1994], whereas GIMMS began with the NOAA/NCAR top of atmosphere (TOA) 15-day data series. GIMMS used NOAA 9 data to fill a 4-month NOAA 11 gap (09/94 to 01/95) while FASIR extrapolated the NDVI record to fill the gap. The processing approaches differ considerably. To produce surface reflectance data corrected for orbital drift over the years, FASIR applied calibration, Bidirectional reflectance function (BRF) and atmospheric corrections (no water vapor) individually to bands 1 and 2 of the cloud-screened Pathfinder AVHRR series of *James and Kalluri* [1994]. To further reduce snow and cloud contamination, Fourier filtering was applied to the NDVI time series and in the tropics spatial aggregation to further mitigate cloud contamination. The GIMMS processing approach did not utilize atmospheric correction, except during the El Chichon and Mt. Pinatubo volcanic stratospheric aerosol periods, and applied corrections to

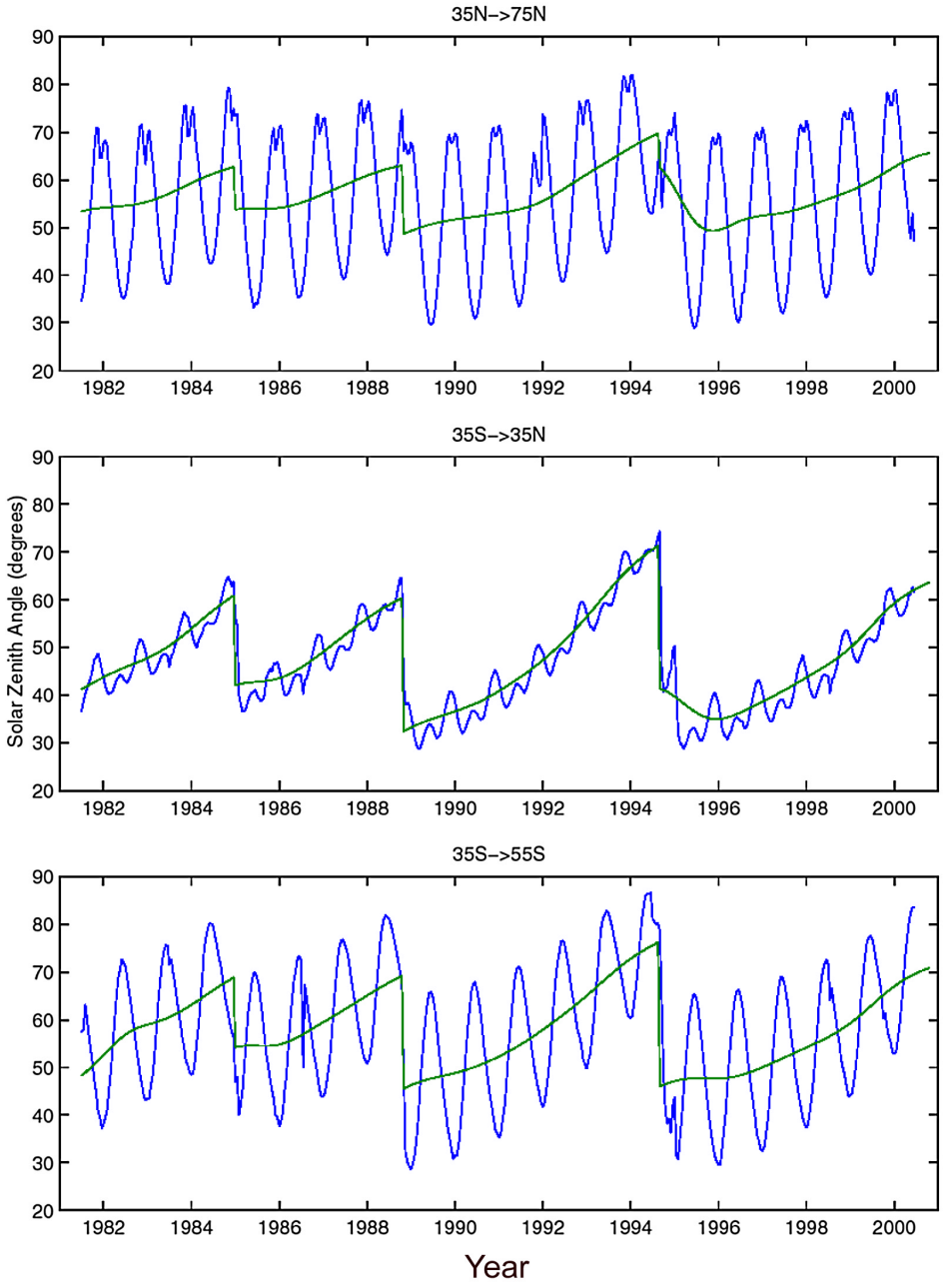

Figure 1. Variation of latitude-averaged solar zenith angle (blue) and trends (green) from NOAA 7 through NOAA 14 for (top) 35 to 75 north latitude; (middle) 35 north to 35 south latitude; and (bottom) 35 to 55 south latitude.

NDVI directly (i.e., does not attempt to correct individual bands). GIMMS used the NOAA thermal band for cloud screening, did not use Fourier filtering to reduce snow and cloud effects and did not use spatial aggregation in the tropics. Hence tropical cloud contamination may be more problematic. GIMMS adjusted the NDVI record for the effects of varying solar illumination angle utilizing the empirical mode decomposition technique [*Huang et al.*, 1998, 1999]. These differences between the GIMMS and FASIR products are discussed more fully in the following sections.

2.1. Data Input

[10] Both FASIR and GIMMS used data composites from the full AVHRR data record but the compositing periods used are somewhat different. Frequent cloud cover eliminates roughly 2/3 of the daily AVHRR record. In order to construct periodic cloud-free views of the Earth, composite monthly images were constructed by selecting for each pixel the maximum NDVI during 10-day (FASIR) or 15-day (GIMMS) intervals. Choosing each pixel's maximum NDVI during an interval of a few days reduces aerosol, cloud cover and water vapor effects since NDVI

Table 1. FASIR and GIMMS Processing Similarities/Differences

	Data Input	Calibration	View/Illum Angle Corr	Atmospheric Corr.	Aerosol Corr.	Other
FASIR Monthly Band 1, Band 2, NDVI	NOAA Pathfinder data set [*James and Kalluri*, 1994]; 10-day composites; corrected for mol scattering. NOAA 11 gap 09/94 to 01/95 filled by interpolation.	NOAA Pathfinder data set after *James and Kalluri* [1994]; additional adjustments using desert calibration targets.	Li Sparse and Ross Thick Kernel [*Wanner et al.*, 1995].	molecular and ozone as per *James and Kalluri* [1994]; not corrected for water vapor; no correction for tropospheric aerosols.	volcanic aerosol corrected Pinatubo 04/82 to 12/84; El Chichon 06/91 to 12/94 [*Sato et al.*, 1993]	CLAVR cloud screen; gap-filled cloudy and missing data.
GIMMS Monthly NDVI only	NOAA/NCAR Top of atmosphere 15-day composites. NOAA 11 gap 09/94 to 01/95 filled with NOAA 9.	*Vermote and Kaufman* [1995] desert calibration; AVHRR NDVI is adjusted higher to match 1997–2003 SPOT NDVI less affected by atmospheric water vapor absorption.	empirical mode decomp.	no explicit atmospheric corrections; however, compositing reduces atmospheric variability; the match to SPOT NDVI reduces the effect of atmospheric water vapor absorption.	volcanic aerosol corrected Pinatubo 04/82 to 12/84; El Chichon 06/91 to 12/94 [*Sato et al.*, 1993; *Vermote et al.*, 1997].	cloud screen using AVHRR thermal band.

is maximum on the clearest days. It should be noted however, that maximum NDVI compositing does not completely remove these atmospheric effects. Compositing can be done over any time interval, but 9 days is generally selected as the minimum period since the NOAA orbit repeats at that frequency. The primary FASIR data record was constructed from 10-day composites. Since ISLSCP contains monthly data, a monthly FASIR data record was generated for the Initiative II collection based on the composite value for days 11–20 because this middle period best represented the entire month. The GIMMS monthly data record is based the average maximum NDVI for each of the 15-day periods in a month.

[11] FASIR NDVI data sets were compiled using band 1, band 2, solar zenith angle, scan angle, and relative azimuth angle values from the Pathfinder AVHRR Land (PAL) data set [*James and Kalluri*, 1994] for the period of 1982–1998. Pathfinder radiances were determined to be more appropriate for FASIR BRF adjustments than top of the atmosphere measurements from the AVHRR sensors because the Pathfinder data set contained band 1 and band 2 radiances corrected for intersensor calibration differences, atmospheric molecular scattering and ozone absorption (from TOMS). Corrections accounted for atmospheric path length changes induced by topographic variations. Pathfinder also cloud screened the AVHRR data using the CLAVR algorithm.

[12] The input data for the GIMMS 1981–2002 time series were the top of the atmosphere NOAA AVHRR GAC 1B data, obtained from NOAA and from National Center for Atmospheric Research (NCAR). GIMMS augmented this data set with GAC 1B data available from NOAA's Satellite Active Archive. Cloud screening was provided by a channel 5 thermal mask of 0°C for all continents except Africa, where a cloud mask of 10°C was used. In addition bimonthly compositing significantly reduced cloud contamination.

[13] The AVHRR acquisitions used for the 1981 to 1998 time period for FASIR and GIMMS are similar, with an important exception. GIMMS utilized NOAA 9 data in the October 1994 to January 1995 period to fill a gap in the Pathfinder record during this period (NOAA 11 started to malfunction and its replacement, NOAA 13, failed shortly after launch; NOAA 14 was not yet launched). During this period, FASIR estimated AVHRR using a climatological mean and the Fourier Adjustment. Specifically, two low-pass filters (±220 day and ±50 day moving windows, respectively) were used to interpolate the missing data for late 1994.

2.2. Data Processing

2.2.1. Calibration

[14] Both GIMMS and FASIR products recalibrated AVHRR band 1 and 2 reflectance measurements to reduce intersensor and intrasensor errors. FASIR started with the calibration procedure of *Rao and Chen* [1994]. This was improved by using a thousand reflectance-invariant sites globally (e.g., deserts) to examine residual variations in Pathfinder band 1, band 2 and NDVI. On the basis of these observations adjustments were made to the *Rao and Chen* [1994] sensor gains to render the band 1 and 2 reflectance more stable over these targets. Following this, the relative RMS error as a result of sensor degradation and intercali-

bration differences in the channel 1 and 2 gains were estimated to be about 1%.

[15] GIMMS used the technique of *Vermote and Kaufman* [1995] to adjust the calibration of NOAA-7 through NOAA-14 AVHRR channel 1 and 2 data. This approach uses a different calibration standard from *Rao and Chen* [1994] and results in slightly higher NDVI values (S. Los, personal communication, 2005). Like FASIR, the calibration was refined using invariant desert sites. The GIMMS data set extends beyond 1998 to include data from NOAA-16. In order to tie together the NOAA-14 and NOAA-16 time series, GIMMS also adjusted the historical (NOAA-14 and earlier) and NOAA-16 NDVI by a constant offset to match up with a coincident and spatially aggregated 8-km SPOT Vegetation NDVI time series. This was necessary because the bilinear gain for channel 1 and channel 2 of NOAA-16's AVHRR instrument complicates ex post facto calibration. It should be noted that calibrating the AVHRR NDVI values to SPOT effectively narrows the instrument band pass, and results in overall higher NDVI values.

2.2.2. NDVI Variations Resulting From Variations in Solar and View Zenith Angle

[16] The FASIR algorithm adjusted for illumination and viewing angle effects in the AVHRR NDVI by estimating the BRF for each pixel from its 17-year variation. This is accomplished by employing the Li Sparse and Ross Thick kernel approach used to estimate MODIS BRF [*Wanner et al.*, 1995]. To obtain sufficient numbers of observations, the BRF for each pixel was assumed constant over the 17-year period so that all monthly NDVI values over the 17 years could be used to estimate the kernels. Using the estimated kernel weights, NDVI was normalized to standard viewing geometry (30 degrees solar zenith angle and 0 degrees view angle). In contrast, GIMMS utilized the empirical mode decomposition (EMD) [*Huang et al.*, 1998, 1999], an empirical approach to correct for view and illumination angle effects. EMD extracts NDVI trends that are more than 80% correlated to the solar zenith angle. Areas with trends that have a lower correlation were not corrected.

2.2.3. Atmospheric Correction

[17] GIMMS applied no atmospheric correction, except during the El Chichon and Mt. Pinatubo volcanic stratospheric aerosol periods. A stratospheric aerosol correction was applied as proposed by *Vermote et al.* [1997] from April 1982 through December 1984 and from June 1991 through December 1994. GIMMS formed composite stratospheric aerosol optical depth fields by combining the work of *Sato et al.* [1993], and *Vermote et al.* [1997]. The work of *Rosen et al.* [1994], *Russell et al.* [1993] and *Dutton* [1994] were used to compare specific optical depth measurements to GIMMS blended global fields. GIMMS optical depth field varied by month and degree of latitude. The Pathfinder data set on which FASIR is based is corrected for atmospheric molecular scattering and ozone absorption, but not water vapor. FASIR also corrected for aerosols injected into the stratosphere by Mt. Pinatubo and El Chichon, but used the aerosol optical depth data from *Sato et al.* [1993]. The *Sato et al.* [1993] data extends further north and south (90 S to 90 N) than the data set by Vermote (50 S to 50 N). Comparison of the NDVI corrected with the Sato and the Vermote optical depth data showed close agreement between 50 degrees South and 50 degrees North. Stratospheric optical depths prior to and 2 years after the eruptions were set to zero for both data sets.

3. Geographic Characteristics

[18] As part of the ISLSCP processing, NDVI data sets were produced at 0.25, 0.50, and 1.0 degree resolution. Original input data for both data sets was the ~4 km resolution NOAA GAC data. The GIMMS NDVI data set was derived directly from this record. The FASIR NDVI data set was derived from the AVHRR Land Pathfinder (PAL) data set, which was resampled to 8 km resolution.

[19] Since NDVI is a nonlinear transformation of the original reflectance data, averaging NDVI from several independent observations across a region will give a different result compared to averaging the original spectral data and then calculating a single, aggregate NDVI value [*Hall et al.*, 1992]. The original NOAA GAC data represent a subsample of the original 1.1 km LAC sensor stream; at nadir only 27% of each 4 km GAC pixel was actually imaged by the instrument [*Townshend*, 1994]. Within the GIMMS processing, these ~4 km NDVI subsamples were mapped to output 8 km grid cells, and the single observation with the maximum NDVI value during the 15-day compositing period was retained. Thus each 64 km^2 15-day GIMMS NDVI value actually corresponds to an irregularly shaped 4.4 km^2 observation from the compositing period; up to 93% of the 8 km cell was not observed by the instrument. For ISLSCP Initiative II, all 8 km GIMMS NDVI values were averaged within a single 0.25 degree grid cell. The FASIR geographic processing approach was similar, except that the compositing period is the middle 10 days of each month, then the 8 km FASIR NDVI values are averaged to form the 0.25 degree output. The differences in compositing procedure imply that each monthly GIMMS 0.25 degree cell at the equator includes information from roughly twice as many AVHRR 1.1 km LAC observations compared to, since two values for each month are incorporated into the GIMMS product, but only one value for the FASIR.

[20] The nature of the FASIR data processing introduced two types of smoothing that are visible in the NDVI data. First, to reduce tropical cloud contamination, FASIR retained the maximum NDVI value from a moving 3 × 3 pixel window for tropical regions. As a result, the nominal resolution of the FASIR data in the tropics is ~24 × 24 km, about the same as the 0.25 degree resolution of the finest ISLSCP grid. Second, the time series from each pixel was fitted with a Fourier representation to identify and remove outliers and create a temporally smooth curve. The removal of outliers also give the FASIR NDVI imagery a smoother, less noisy appearance compared to GIMMS data.

[21] Overlaying the Initiative II GIMMS and FASIR data sets at 0.25 degree resolution indicates a systematic misregistration of about 1/2 pixel (~13 km at the equator), with the FASIR data offset to the southwest compared to the GIMMS. To evaluate which data set is correctly registered, orthorectified (<60 m 1σ geodetic accuracy) Landsat TM imagery from the Nile river was compared with the two NDVI data sets within ArcGIS. The Nile river offers a useful registration target given the sharp boundary between the vegetated valley and delta, and the unvegetated desert

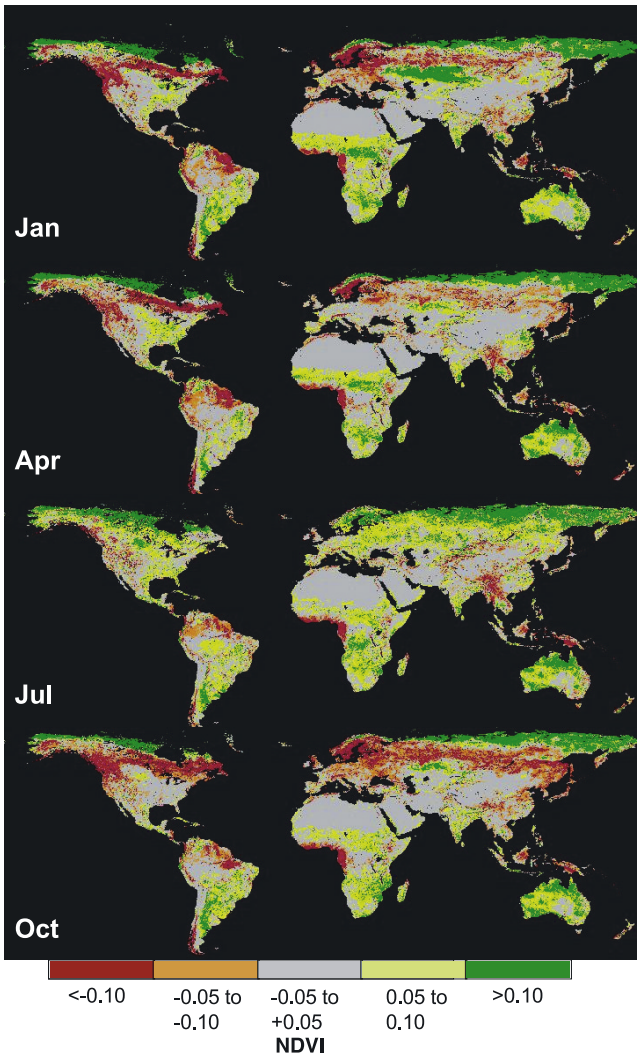

Figure 2. Absolute difference in average monthly NDVI between GIMMS and FASIR data sets for January, April, July, and October. The length of record in each case was 1983–1998.

surroundings. Comparing the boundaries of the vegetated zone mapped from the Landsat suggests that the GIMMS data set is correctly registered, while the FASIR data is misregistered (to the southwest).

4. Comparisons of GIMMS, FASIR NDVI Absolute Values

[22] As noted above, the processing approaches of the FASIR and GIMMS NDVI data sets are quite different in philosophy and approach. In comparing absolute NDVI values between the products it is useful to consider how these processing choices have affected the NDVI measurement.

4.1. Calibration and Scaling

[23] Although both FASIR and GIMMS used desert calibration targets, they used slightly different calibration methodologies. The GIMMS calibration approach results in a small offset (bias) of NDVI by ~0.05 (S. Los, personal communication, 2005). In addition, the GIMMS applies a scaling factor to match the NDVI derived from the SPOT Vegetation sensor data during the 1997–2003 period of observational overlap. The much narrower band pass of SPOT Vegetation compared to AVHRR was designed to avoid atmospheric water vapor absorption in the NIR band, hence SPOT NDVI will be larger than that calculated from AVHRR; hence scaling the GIMMS with the SPOT product increases the GIMMS NDVI amplitude.

4.2. Atmospheric Correction

[24] GIMMS and FASIR NDVI represent fundamentally different measurements of the land surface. Although NDVI is commonly defined in terms of surface or top of atmosphere reflectance, neither the GIMMS nor FASIR records implemented a full atmospheric correction. GIMMS was corrected only for stratospheric aerosols. FASIR NDVI included ozone and Rayleigh corrections, but not tropospheric aerosols or water vapor. In general, the Rayleigh scattering correction implemented by FASIR should result in lower reflectance in the AVHRR visible band for dark vegetated targets, and hence higher NDVI values compared to the TOA GIMMS product.

4.3. Surface BRDF Correction

[25] The FASIR data have been BRF corrected to nadir look angle, and 60 degree solar elevation [*Los et al.*, 2005] whereas GIMMS NDVI values were measured at a range of view angles selected by compositing. The BRF adjustment may increase NDVI calculated from TOA or surface reflectance, particularly in conditions of high aerosol optical thickness [*Los et al.*, 2005]. The effects of the BRF correction are more pronounced in forests (owing to multiple scattering of near-infrared radiation in the canopy), and at high latitudes in the winter when the observed solar elevation is low.

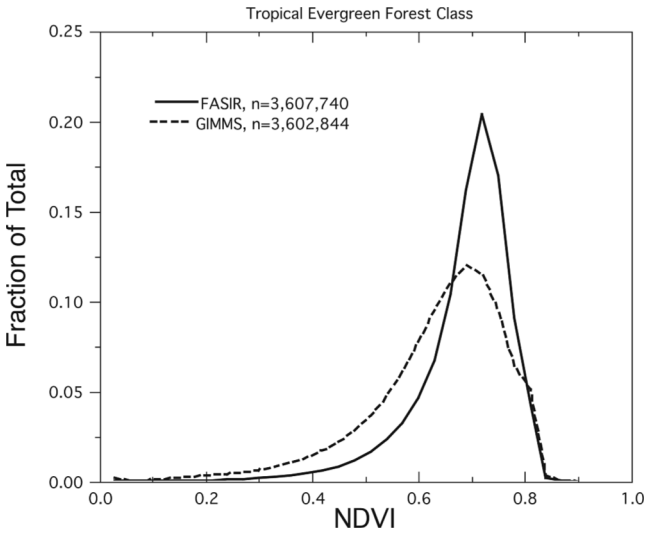

Figure 3. Distribution of NDVI values for tropical evergreen forest for all months in the 1982–1998 period, derived from ISLSCP II 0.25 degree EDC Landcover classification and the 0.25 degree FASIR and GIMMS data sets.

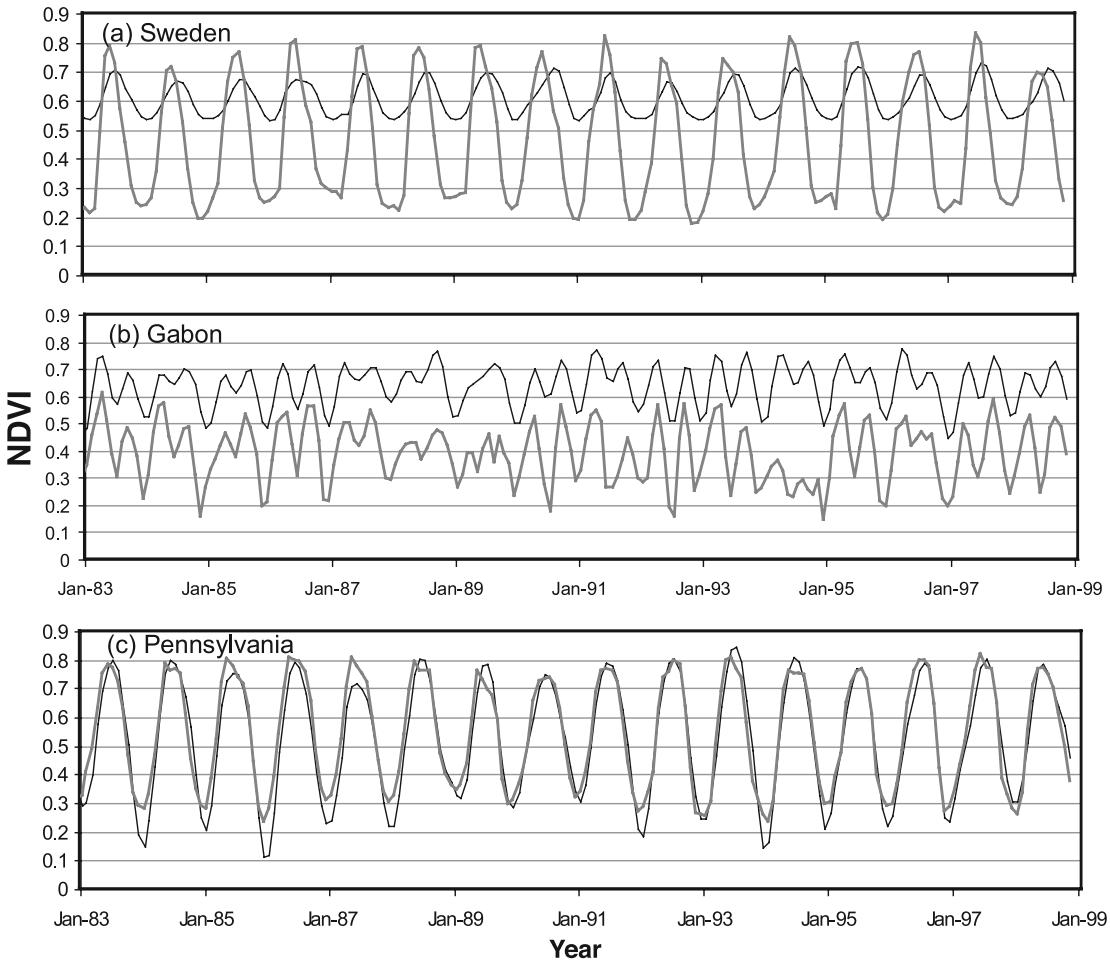

Figure 4. Time series of NDVI values from FASIR (thin black line) and GIMMS (thick grey line) for (a) Sweden, (b) Gabon, and (c) Pennsylvania.

4.4. Filtering and Interpolation

[26] As noted above, the FASIR used filtering and interpolation methods not employed in GIMMS. FASIR replaced NDVI values in the tropics with the maximum of a 3 × 3 pixel moving window to actively suppress cloud contamination, thus tending to raise NDVI values. In the Boreal forests (northern conifers) FASIR replaced low winter NDVI values with the median October value to avoid snow contamination, thus producing a higher winter NDVI in this biome. Finally, the FASIR Fourier filtering will tend to remove individual outliers, whether very high or very low.

[27] Given these processing differences, it is not surprising that absolute NDVI values of the two data sets show strong and consistent mismatches. The differences between the FASIR and GIMMS monthly average NDVI are shown in Figure 2. Slightly over half of the globe's land area shows good agreement (<0.05 absolute NDVI difference) between the two data sets. These areas tend to be those with limited NDVI values (e.g., hyperarid regions in North Africa and Arabia) or range (Western Amazon and Central Africa). In general, FASIR NDVI is considerably higher in the cloudy tropics (e.g., West Africa, Guyana, Myanamar, New Guinea), reflecting the effect of the FASIR 3 × 3 maximum NDVI filter. This filter was implemented to reduce cloud contamination but will also result in higher NDVI in clear areas. As a result, NDVI values in these areas range from 0.5–0.7 in the FASIR data set, but just 0.3–0.5 in the GIMMS data set (Figures 3 and 4b). On the basis of comparisons with Landsat TOA and surface reflectance imagery, NDVI values for tropical forests should be considerably higher than those represented in the GIMMS record, despite the lack of atmospheric correction in GIMMS. Though the maximum NDVI values for evergreen tropical forest type for all months of the data record are similar between the two data sets, FASIR has more observations at high NDVI values while GIMMS shows a broader distribution of NDVI values (Figure 3).

[28] Except for the midsummer, northern temperate and boreal forests tend to exhibit considerably higher NDVI in FASIR than GIMMS (Figures 2 and 4a). This can be explained through three contributing factors. First, the Rayleigh and ozone corrections applied to the FASIR data tend to increase NDVI, by reducing path radiance in the AVHRR visible band. Second, the FASIR BRF correction tends to increase NDVI in Winter, Fall, and Spring. Finally, the filtering applied to the FASIR record replicates the October NDVI value in boreal regions during the winter to eliminate snow contamination, resulting in higher values compared to GIMMS. During the midsummer the situation

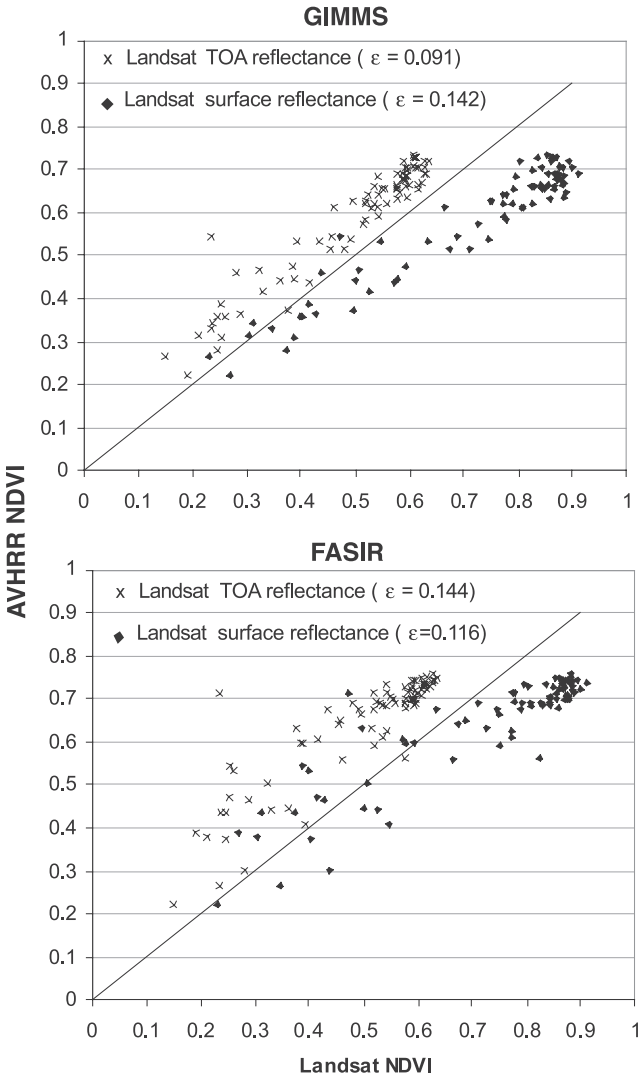

Figure 5. Comparison of Landsat-derived NDVI values (averaged over 0.25° ISLSCP Initiative II grid) with (top) GIMMS and (bottom) FASIR values, for Montana/Idaho region. Landsat data are from WRS-2 path 42, rows 27–28 acquired 10 September 1990. GIMMS and FASIR data are from September 1990 maps. Landsat NDVI calculated from both top-of-atmosphere reflectance (crosses) and atmospherically corrected surface reflectance (diamonds) are shown.

reverses, with GIMMS NDVI data trending significantly higher at latitudes north of ~50 degrees N. At 60N, the GIMMS NDVI values are up to 0.20 greater than FASIR. Since FASIR is not corrected for water vapor effects in band 2, this probably reflects the postcalibration scaling of GIMMS to the higher TOA values of SPOT Vegetation NDVI (its IR band largely avoids the water vapor absorption line), which tends to amplify the NDVI difference over the seasonal NDVI cycle.

[29] Southern hemisphere grasslands, shrublands, and semiarid environments tend to show higher values in the GIMMS data set than in FASIR, at all times of year. For example, values in Western Australia and Queensland are up to 0.20 higher in the GIMMS record, and values in the Argentine Pampas are up to 0.16 higher. Results of *Los et al.* [2005] suggest that BRF correction for grasslands (in North America) tend to reduce FASIR NDVI values during peak greenness, which could explain some of the offset. However, it is not clear why this difference should persist throughout the year.

[30] Despite these differences, in many parts of the world the NDVI values in the two data sets do agree. For example in North Africa (where both data sets were calibrated prior to atmospheric correction) NDVI differences are typically less than 0.03. In temperate regions of the Northern Hemisphere (e.g., central and eastern United States, central Europe, southern Russia, China) differences are usually less than 0.05 (Figures 2 and 4c).

[31] To investigate differences between the data sets more fully, we have processed several Landsat TM scenes from the 1980s and 1990s to both surface and TOA reflectance using the 6S radiative transfer model [*Vermote et al.*, 1997; *Masek et al.*, 2006]. Because the Landsat data represent instantaneous, cloud-free views, NDVI retrieved from Landsat avoids errors associated with compositing and cloud clearing. Landsat NDVI was calculated from red and near-infrared (band 3 and 4) reflectance values, and then averaged to the 0.25° resolution of the ISLSCP Initiative II grid. The Landsat TM band passes are substantially narrower compared to the AVHRR band pass, and one could in principle adjust the Landsat measurements to "match" the AVHRR NDVI. Here we have not elected to do so, in part because the GIMMS data is already normalized to the narrow band pass of the SPOT Vegetation sensor.

[32] A transect across western Montana and Idaho includes a range of vegetation conditions at midlatitudes, including dense conifer forest, sparse woodlands, semiarid shrublands, and agriculture. Two successive Landsat acquisitions from 10 September 1990 provide 79 quarter degree observations for comparison with the ISLSCP data sets (Figure 5). The GIMMS record shows a strong correlation with the Landsat NDVI values. As expected, the GIMMS data (derived from AVHRR TOA reflectances) most closely matches the Landsat TOA NDVI, on the basis of the lower average absolute difference between values (Figure 5). The correlation with FASIR data over the same region is slightly weaker, with greater dispersion of low NDVI values, but a closer association with the Landsat surface reflectance NDVI.

[33] A second, north-south transect was analyzed to examine differences between FASIR and GIMMS in Boreal midsummer conditions (Figure 6). This transect (July 1991) includes data from 98.75–99.00 degrees west, and extends from 80 degrees north (Northwest Territories, Canada) to 45 degrees north (South Dakota, United States). As noted above, GIMMS and FASIR values appear consistent in the midcontinent but diverge in Boreal regions, with GIMMS having consistently higher values in midsummer. A set of Landsat NDVI values from July 1991 are also plotted (path 35, rows 17–18, acquired July 26, 1991). In contrast to the Montana example, the GIMMS data in this case show far higher values than that found for Landsat TOA NDVI, and are even higher than Landsat surface reflectance NDVI.

[34] It is clear from these analyses and comparisons between the FASIR and GIMMS NDVI records, that neither can be used in an absolute sense, since neither completely

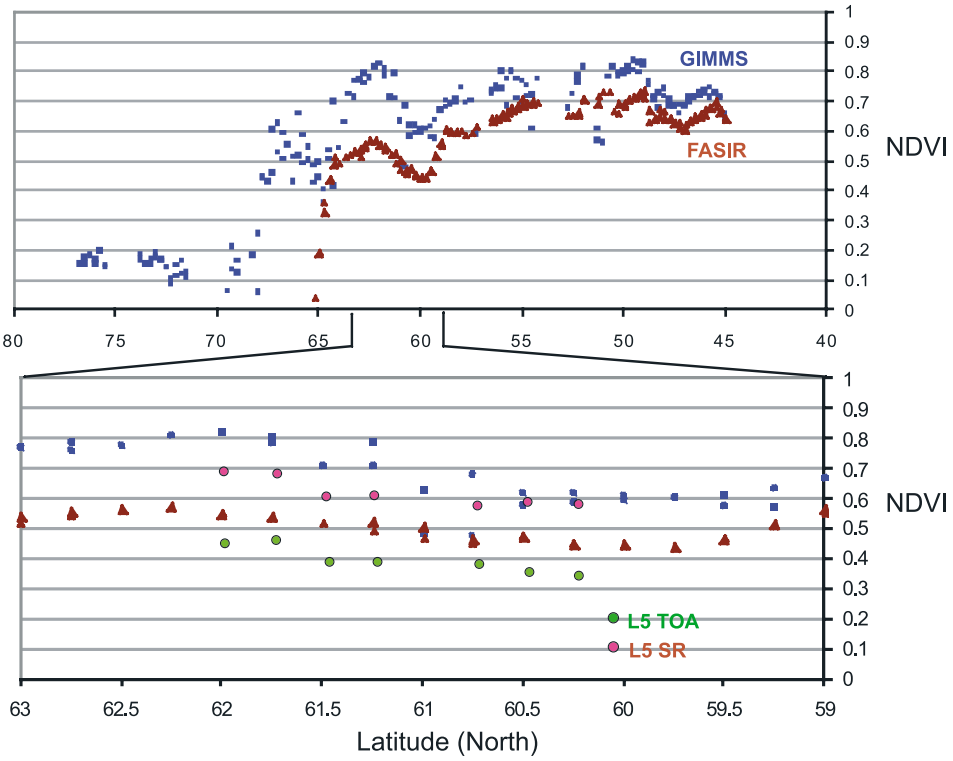

Figure 6. (top) North-south transect near 100 degrees W longitude, from Northwest Territories, Canada, to South Dakota, United States. Both GIMMS (blue square) and FASIR (red triangle) NDVI data are shown. (bottom) Expanded version GIMMS (blue square) and FASIR (red triangle) extending from 59 to 63 degrees North, with averaged Landsat NDVI observations superposed, based on top-of-atmosphere reflectance (green) and surface reflectance (red).

corrects for spatial or seasonal atmospheric variations, particularly tropospheric aerosols and water vapor, which themselves can have a strong seasonal signal. Alternatives to using the absolute values are discussed and evaluated further in the next section.

5. Interannual Variability of NDVI Anomalies

5.1. Interannual NDVI Patterns

[35] Both FASIR and GIMMS NDVI data records exhibit variability resulting from calibration, viewing geometry and atmospheric conditions that alter the land surface reflectance signal inferred from the satellite observations. Recognizing this some analyses of long-term trends in vegetation greenness [*Myneni et al.*, 1997; *Zhou et al.*, 2003] or drought response [*Anyamba et al.*, 2001; *Ji and Peters*, 2003] rely on the use of NDVI anomalies, i.e., the deviation of NDVI measurements in a record from the average monthly or annual NDVI computed from that record. Ideally, interannual anomalies should match across the FASIR and GIMMS records, even if absolute NDVI values differ.

[36] In Figure 7 we show the NDVI anomalies for continental regions of the globe. Not only are there differences in the absolute NDVI records shown in Figures 2 through 6, there are also significant differences in the two anomaly records that are of similar magnitude to the annual anomalies themselves. The anomalies in the FASIR record and the difference between FASIR and GIMMS are especially large in the period 1984–1986 and in 1994 for all continental regions. In addition, FASIR NDVI data tend to show much stronger negative anomalies compared to GIMMS for 1992. This difference is possibly a result of different stratospheric aerosol optical thickness data sets used in GIMMS and FASIR. Both data sets show positive trends for North America, Europe and Asia, while only FASIR shows a positive trend for Africa and both data sets show no trends for Central/South America and SE Asia/Australia. The regional correlation coefficients for the NDVI anomalies are shown in the figure. Correlations are generally poor (and not statistically significant) except for Europe and Asia (>99%). The correlation between the anomalies for boreal North America is high but poor for temperate North American (not shown) producing a low correlation for the continent.

[37] The 1994 disparity is largely a result of the different FASIR, GIMMS approaches dealing with the NOAA 13 failure between NOAA-11 and NOAA-14 as discussed in section 2.1. The anomalies are more similar during the rest of the time series for northern latitude continental regions.

5.2. Evaluation and Comparison of the Initiative II NDVI Series in the Context of Carbon Cycle Modeling

[38] To determine which NDVI time series might be more realistic, we use both the GIMMS and FASIR NDVI time

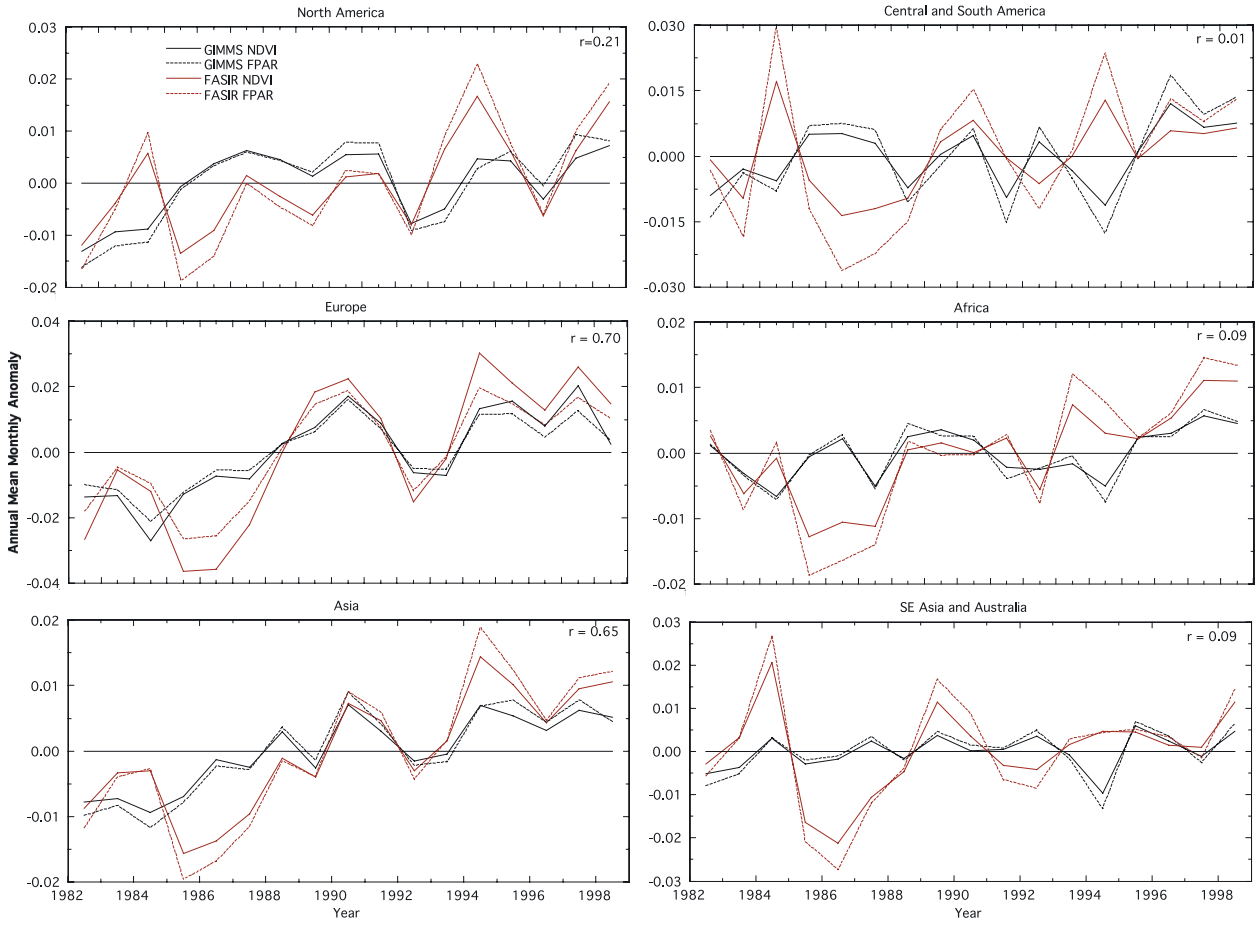

Figure 7. Time series plots showing annual GIMMS NDVI and fPAR anomalies (black solid, dashed lines, respectively) and FASIR NDVI and fPAR anomalies (red solid, dashed lines, respectively) for continental regions of the globe. Correlation coefficients (r) are given for NDVI anomalies.

series as input to a global carbon cycle model, CASA, that simulates the surface-atmosphere exchange of CO_2 [*Potter et al.*, 1993; *Randerson et al.*, 1996] (and described briefly in the next section) to explore these implications. CASA uses fPAR, derived from the NDVI record (as described in the next section) and surface incident solar irradiance to compute photosynthetically active radiation absorbed by the canopy, and uses temperature and precipitation data to compute light use efficiency and heterotrophic respiration. Using CASA we predicted global interannual variation in net land surface-atmosphere carbon exchange and compare these values to those estimated from an atmospheric CO_2 flux inversion study.

5.2.1. Approach

[39] CASA uses the light use efficiency approach [*Monteith*, 1997] to characterize climate-induced deviations in productivity capacity. Monthly global ($1^\circ \times 1^\circ$) net primary productivity (NPP) is calculated as the product of incident photosynthetically active radiation (PAR), and its fraction absorbed by the canopy (fPAR) and a light use efficiency parameter, the latter dependent on temperature and precipitation (for temperature, precipitation and solar irradiance data, see *Hansen et al.* [1999], *Adler et al.* [2003], and *Zhang et al.* [2004], respectively). Heterotrophic respiration is computed using temperature and precipitation data and also depends on modeled NPP. To convert NDVI into fPAR we implemented the algorithm reported by *Los et al.* [2000] in which NDVI is used to scale fPAR from some minimum value (<0.05), corresponding to the minimum NDVI observed for vegetation, to a maximum (0.95) representing the maximum (e.g., 98th percentile) observed NDVI, hence full canopy closure. The scaling is dependent on maximum and minimum NDVI observed for various vegetation types (e.g., Figure 3). The derivation of fPAR "normalizes" the NDVI record allowing the FASIR and GIMMS anomaly records to be evaluated in a consistent way.

[40] Since the dynamic range of NDVI is higher for the FASIR than for GIMMS data sets the maximum/minimum scalars used for each data set reflected these differences, but were in fact small and showed consistent relationships among the vegetation types. Figure 7 shows the NDVI and fPAR annual anomalies for continental regions from 1982–1998. Each continental region consists of a number of vegetation types. The sign of the anomalies in NDVI correspond to those for fPAR, only the dynamic range of the fPAR is larger since NDVI ranges between ~0–0.8 while fPAR ranges from ~0.03–0.95.

[41] Using the calculated GIMMS and FASIR fPAR records and climate data, we ran CASA to simulate NPP, heterotrophic respiration (Rh) and the net flux to the

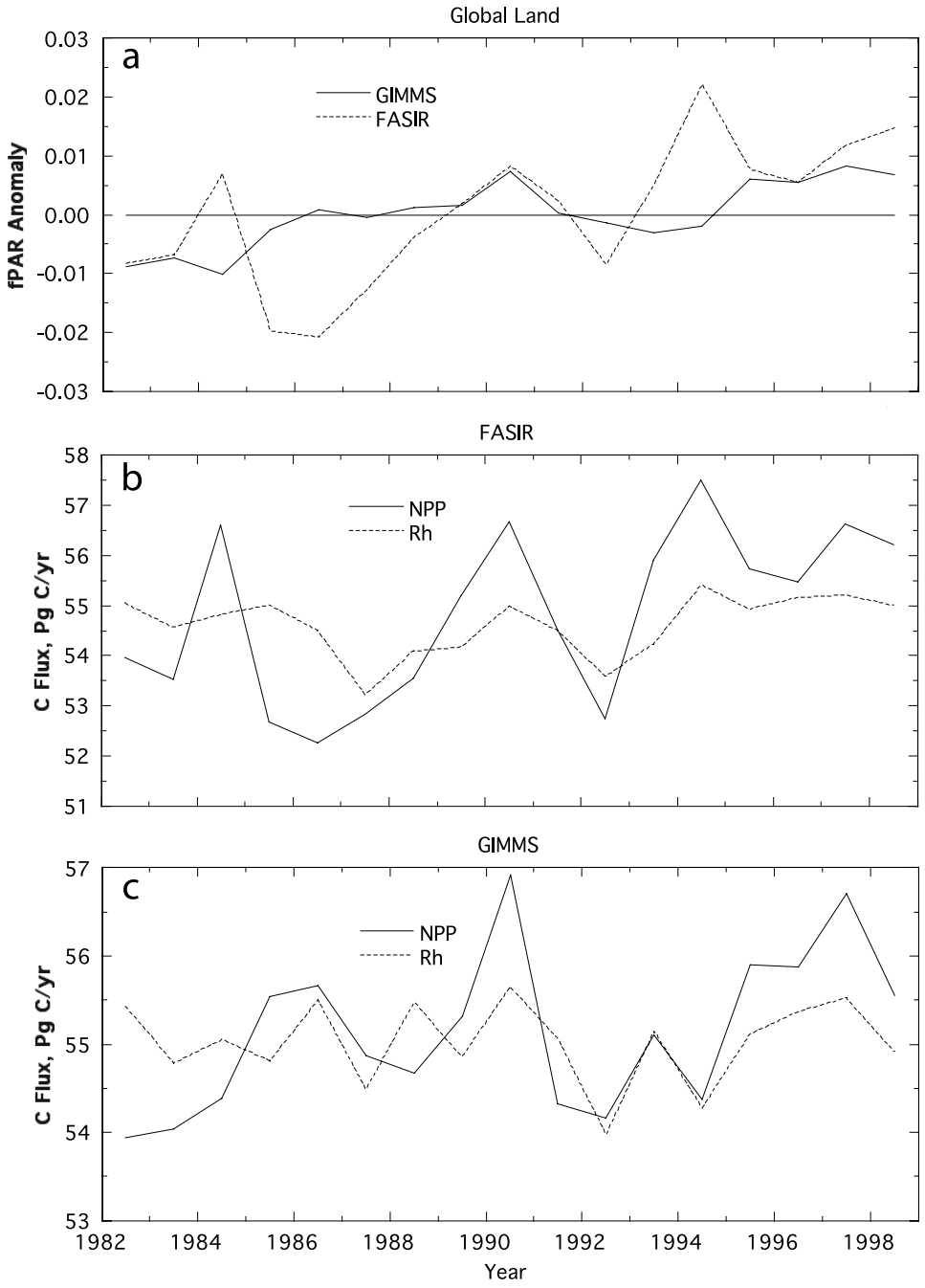

Figure 8. Global fPAR anomalies and carbon fluxes from CASA: (a) annual fPAR anomalies for the globe calculated from GIMMS (solid line) and FASIR (dashed line) NDVI records; (b) global net primary production (NPP) and heterotropic respiration (Rh) fluxes calculated from observed climate record, using the CASA biogeochemical model driven with FASIR NDVI/fPAR anomalies; and (c) same as Figure 8b, except driven with GIMMS NDVI/fPAR anomalies.

atmosphere (Rh-NPP or NEE). We have aggregated the results to represent global land area. CASA was run to equilibrium (annual NEE = 0 for each grid cell) using the mean climate and fPAR for the 1982–1998 period and then the interannual simulation was started and run forward from January 1982 through December 1998 using observed time series of fPAR and climate inputs. Figure 8a shows the annual fPAR anomalies for the globe and Figures 8b and 8c the NPP anomalies for FASIR and GIMMS respectively. The larger range of the FASIR NDVI, hence fPAR, is reflected in the range of NPP. NPP is largely driven by fPAR in the CASA model with weaker effects from lower variability in incident solar irradiance, and lower sensitivity to temperature and precipitation. A 0.01 change in the annual fPAR anomaly translates to about 1.5 Pg C/yr NPP anomaly which means that a 0.01 change in the original NDVI corresponds to about 2 Pg C/yr change in NPP. The largest year-to-year NPP anomalies using FASIR as the input

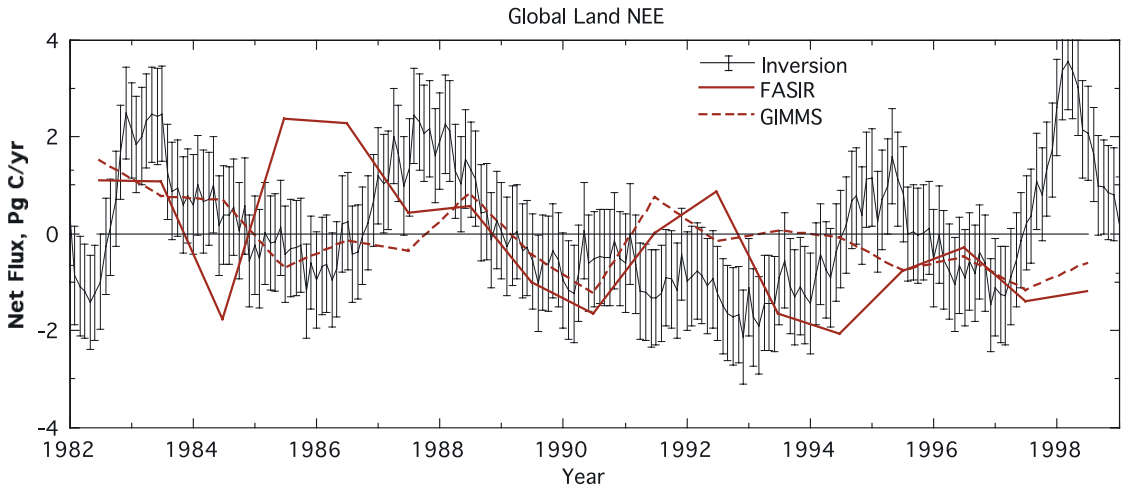

Figure 9. Global net ecosystem exchange (NEE) simulated by CASA using FASIR and GIMMS records plotted with observed global fluxes derived from atmospheric carbon flux inversion of *Rödenbeck et al.* [2003]. The mean land carbon sink of 1.5 PgC/yr for this period was added to the inversion results to emphasize the comparison of interannual variability between the inversion and CASA simulations. Positive NEE corresponds to carbon transfer from the land to the atmosphere (e.g., land CO_2 source); NEE is calculated as Rh-NPP.

to CASA were about 3 Pg C/yr and generally <2 Pg C/yr using GIMMS. Also plotted in Figures 8b and 8c are Rh anomalies. In CASA Rh is determined by temperature and precipitation controls on 9 carbon pools with varying turnover times. However, since the same climate was use for both CASA runs the differences in Rh are a result of NDVI/fPAR-driven NPP variability. A large NPP anomaly will result in a significant anomaly in the delivery of carbon to heterotrophic carbon pools some of which have turnover times of less than 1 year (e.g., leaf and root litter).

5.2.2. Simulation Results and Comparisons

[42] Figure 9 shows the difference between Rh and NPP or NEE, the flux of carbon between the surface and atmosphere. When it is positive it represents a source to the atmosphere and negative a sink. Included in the figure are the results of an atmospheric inversion study [*Rödenbeck et al.*, 2003] where land sources and sinks were inferred from a model of atmospheric transport and surface measurements of atmospheric CO_2 partial pressure from a global sampling network. The error bars represent 1 standard deviation about the mean. The fossil fuel source has been "presubtracted" from the inversion results. The original inversion results showed that the global land surface to be on average for this period a carbon sink of about 1.5 Pg C per year for. In Figure 9 this constant 1.5 Pg C sink was added to the inversion results since the CASA simulations, were initialized to produce an equilibrium NEE (i.e., NEE = 0) at the 1982 start of the evaluation period. CASA simulations show a trend of increasing sink over the time period that is not evident in the inversion.

[43] The inversion produces maximum year-to-year variability of about 2–3 Pg C/yr. The Transcom inversion study [*Baker et al.*, 2006; K. Gurney, personal communication, 2005] inferred maximum variability of around 3 Pg C/yr as well, however, *Bousquet et al.* [2000] reported maximums of around 1.5 Pg C/yr. The CASA simulations produced maximum variations of about 1 and 3 Pg C/yr for GIMMS and FASIR respectively. However, the CASA model results do not produce the same timing in the anomalies as the inversion. In fact for some periods the anomalies are of opposite sign. For instance, the FASIR driven simulations produced strong source anomalies in 1985–1986 and 1992 while the inversions show these to be periods of neutral or significant sink behavior. With the exception of 1983 neither of the NDVI driven simulations produced the strong source signals seen in the inversion during the El Ninos of 1987, 1994–1995 and 1998.

5.2.3. Discussion

[44] Our analysis in the previous section indicates little correspondence between either the FASIR NDVI or the GIMMS NDVI anomaly records and the global land source/sink variability inferred from atmospheric inversion; nor do the CASA simulations of NEE when driven by either FASIR or GIMMS NDVI. Assuming that the climate data used to drive the model and the inversion results for the global land are correct, this lack of agreement could be caused by errors in the NDVI records and/or errors and omissions in the modeling of NEE.

[45] In general, NEE can be described by the following equation:

$$\mathrm{NEE} = \mathrm{Rh}(\mathrm{T},\theta) + \mathrm{E} - \int_{\mathrm{t}} \{\varepsilon(\mathrm{T},\theta) * \mathrm{fPAR} * \mathrm{PAR}\}\mathrm{dt}.$$

The product of the last three terms (in brackets) describes NPP: PAR and fPAR defined in 5.2.1 (fPAR is derived observationally from NDVI) records the relative amount of radiation absorbed by the canopy, and ε is the light-use efficiency of vegetation as a function of temperature (T) and soil moisture (θ). The first two terms describe offsetting transfers of carbon to the atmosphere. Rh describes heterotropic respiration of biomass debris (leaves, roots,

soil organic matter), and E corresponds to nonphysiological carbon emissions mostly due to biomass burning. The individual contributions of NPP, Rh or fire to the atmospheric CO_2 signal can be of opposite signs, and compensating, hence only the aggregate effect, not the individual contributions, is reflected in the atmospheric CO_2 inversion analyses. The version of CASA used here simulates only the first two processes (but see *van der Werf et al.* [2004]).

[46] At a minimum, it is clear that the Initiative II NDVI anomaly records alone cannot explain the global atmospheric CO_2 variability derived from the inversion analyses. In CASA, the observed variability in NDVI translates directly to variations in fPAR, which in turn cause large swings in NPP. Since variability in Rh is influenced by short-term pools of accumulated carbon as well as climate Rh will also respond in parallel with NPP to fPAR.

[47] One possibility is that the NDVI records are correct, and other factors not accounted for in CASA compensate for the effects of fPAR variability on global NEE. First, fire emissions may dominate variability of atmospheric CO_2 fluxes. A number of researchers have argued that fires associated with El Nino events contribute significantly to increased atmospheric CO_2 growth rate during these periods [*Langenfelds et al.*, 2002; *Schimel and Baker*, 2002; *van der Werf et al.*, 2004], and *van der Werf et al.* [2004] estimated that fires contributed a 2.1 PgC/yr growth rate anomaly during the 1997–1998 El Nino. If these fire emissions were added to the CASA simulations shown in Figure 9, most of the inversion fluxes would be captured for that period.

[48] In addition to fire, others have suggested that climate controls on light-use efficiency or heterotrophic respiration may act as a primary forcing on CO_2 fluxes. *Nemani et al.* [2003] showed a negative correlation between global atmospheric growth rate in CO_2 and modeled NPP during the large El Nino event of 1997–1998. NDVI tended to show positive anomalies for that period (see Figures 8 and 9), but in their model, physiological drought reduced NPP. Other analyses have shown similar drought limitations on productivity and/or temperature stimulation of respiration [*Tian et al.*, 1998; *Zeng et al.*, 2005]. *Lucht et al.* [2002] showed that negative anomalies in modeled LAI in the boreal latitudes in 1992 following the Mt. Pinatubo eruption corresponded to negative anomalies in NDVI yet their model produced a carbon sink in this region, which was in agreement with atmospheric inversion results. While in their model decreasing LAI did result in a decrease in modeled NPP, the cooler summer temperatures inhibited modeled Rh even more resulting in the net sink. It should be noted that the version of CASA used in this analysis includes temperature and moisture scalars designed to simulate climate effects on vegetation physiology and heterotrophic respiration. However, it is certainly possible that CASA is currently underestimating these effects.

[49] Finally, it is also possible that the NDVI anomalies themselves are wrong. Large interannual anomalies in fPAR, as suggested by the Initiative II data sets, imply significant anomalies in the seasonal duration of canopy LAI and/or its seasonal maximum, both of which would affect annual productivity anomalies [*Barr et al.*, 2004]. Unfortunately there are few in situ measurements of interannual variability of fPAR/LAI against which to assess whether the fPAR variability inferred from the NDVI records is valid. *Barr et al.* [2004] reported strong links between interannual variability in LAI, GPP and NEE for a deciduous boreal forest (aspen), where LAI variations were driven primarily by spring temperature and by summer drought. The interannual variability in fPAR derived from their in situ–measured LAI were on the order of 0.03 and consistent with the anomalies derived from the Initiative II NDVI records. Seasonal and interannual variability of LAI in herbaceous vegetation types especially in response to water availability is well documented and these have been linked to productivity and NEE variability [e.g., *Flanagan et al.*, 2002], but contributions of nonforested ecosystems to interannual variations in carbon storage should be small because the biomass of these systems has short turnover times and most of the fixed carbon is returned to the atmosphere each year. We have not been able to find studies of interannual variability in fPAR/LAI measured in situ in evergreen forest types (e.g., boreal, tropical). These ecosystems are critical to global carbon cycling, but also problematic for NDVI estimation because of the short growing season for Boreal forests and persistent cloud cover in the tropics.

[50] We cannot conclude that our NDVI records, either FASIR or GIMMS, are incompatible with the inversion analyses. However, we can caution researchers that using observational NDVI alone to estimate carbon fluxes is unlikely to match atmospheric measurements. Either the NDVI records themselves are in error, or the contribution of fPAR variability to the interannual variation in NEE is small in comparison to climate-induced interannual variations in light use efficiency, Rh, or fire emissions. Our analyses of the Initiative II NDVI time series also indicate the need for continued improvement in the longer-term satellite derived surface vegetation records including in situ validation, along with improved sampling of atmospheric CO_2 variations and improved transport models supporting inversion analyses.

6. Conclusions

[51] In this paper we have compared the FASIR and GIMMS AVHRR NDVI data sets included in ISLSCP Initiative II [*Tucker et al.*, 2005]. Although both data sets start by compositing the AHVRR GAC record, each processing stream is unique. The FASIR data set attempts a series of physically based corrections to the original AVHRR data set, including atmospheric correction (Rayleigh and ozone), BRDF correction to standard sun-target-sensor geometry, and time-space filtering to remove snow and cloud contamination. The GIMMS data set adopts a more empirical approach, eschewing full atmospheric correction, and relying on empirical-mode decomposition to remove outliers, and normalizing NDVI values to the later SPOT Vegetation record.

[52] Our principal conclusions are as follows.

[53] 1. Absolute NDVI values differ considerably between the two data sets, both seasonally and geographically. Most of these differences are persistent across the 12 year record considered here, and can be understood as the result of specific processing choices. In particular, NDVI values in the humid tropics are systematically lower in the GIMMS record, while nonsummer values in northern latitudes are

systematically higher in the FASIR record. NDVI values in midlatitude deserts and agricultural areas generally agree between the two records.

[54] 2. As opposed to absolute values, NDVI anomalies (monthly, annual) generally agree between the two data sets for any given location. Agreement is better for later parts of the record (e.g., 1992–1998). Two notable exceptions are 1994 and 1984–1986. The former corresponds to the coverage gap between NOAA-11 and NOAA-14, during which the two records rely on different data sources. The origin of the 1984–1986 anomaly disagreement is not clear.

[55] 3. The fPAR absorbed by vegetation calculated from each record closely follows the NDVI anomalies, and shows large interannual variations. Using a standard light-use efficiency model for calculating net primary productivity (NPP), we find that global anomalies of ~0.010 in NDVI correspond to anomalies of ~0.013 in fPAR, and an NPP anomaly of ~2.0 Pg C.

[56] 4. Using the NDVI records to drive the CASA biogeochemical model results in global carbon fluxes that show little or no correlation with sources and sinks derived from inverting atmospheric CO_2 measurements [*Rödenbeck et al.*, 2003]. Although the fPAR-driven fluxes show year-to-year variations comparable in magnitude to the inversion results, neither NDVI record produces a temporal pattern that matches the inversion results.

[57] Users should not rely on absolute NDVI values, particularly in the context of physical models. Although it would be difficult to find a simpler spectral index than NDVI, the processing chain required to convert AVHRR observations to a consistent surface NDVI record is complex and at this date, incomplete. As a result the FASIR NDVI and GIMMS NDVI records must be treated as different measurements. In part this situation reflects the inherent limitations of the AVHRR sensors, which were never intended for long-term terrestrial research. It can be hoped that future NDVI data sets, using carefully calibrated, screened, and atmospherically corrected data from MODIS and VIIRS, will result in a more consistent record of Earth's vegetation. Even with the current limitations of the AVHRR observational record, monthly and annual NDVI anomalies show reasonable agreement between the FASIR and GIMMS, suggesting that users should try to use normalized (anomaly) NDVI values rather than absolute values.

[58] The observation that neither NDVI data set can be correlated with observed carbon fluxes has significant implications for carbon modeling. Taken at face value, the CASA model results, driven by the NDVI anomaly record, predict large variations in vegetation fPAR and LAI that are not driving variability in global carbon fluxes. It is of course possible that CASA and/or the NDVI anomaly records are wrong. Other factors that may not be adequately represented in this version of CASA, such as the physiologic response to climate stress or fire emissions, could be compensating for real variations in NDVI/fPAR. Alternatively, large anomalies in NDVI/fPAR may not be real. Indeed, it is likely that modeling ecosystem productivity using a simple "climatological" mean fPAR record, supplemented with ENSO-driven fire emissions would produce a reasonable match to the inversion results shown in Figure 9. The results do indicate that researchers should be cautious when using NDVI-driven models to predict net ecosystem exchange without independent comparison with observed fluxes.

[59] **Acknowledgments.** This study was supported by NASA's Hydrology and Terrestrial Ecology Programs as well as by a NASA REASON Cooperative Agreement, We thank Christian Rödenbeck for providing us with the atmospheric inversion data. Fred Huemmrich is thanked for analysis of the effects AVHRR and Landsat band passes.

References

Adler, R. F., et al. (2003), The Version 2 Global Precipitation Climatology Project (GPCP) monthly precipitation analysis (1979–present), *J. Hydrometeorol.*, *4*, 1147–1167.

Anyamba, A., C. J. Tucker, and J. R. Eastman (2001), NDVI anomaly patterns over Africa during the 1997/98 ENSO warm event, 2001, *Int. J. Remote Sens.*, *22*, 1847–1859.

Asrar, G., M. Fuchs, E. T. Kanemasu, and J. L. Hatfield (1984), Estimating absorbed photosynthetic radiation and leaf area index from spectral reflectance in wheat, *J. Agron.*, *76*, 300–306.

Baker, D. F., et al. (2006), TransCom 3 inversion intercomparison: Impact of transport model errors on the interannual variability of regional CO_2 fluxes, 1988–2003, *Global Biogeochem. Cycles*, *20*, GB1002, doi:10.1029/2004GB002439.

Barr, A. G., T. A. Black, E. H. Hogg, N. Kljun, M. Morgenstern, and Z. Nesic (2004), Inter-annual variability in the leaf area index of a boreal aspen-hazelnut forest in relation to net ecosystem production, *Agric. For. Meteorol.*, *126*, 237–255.

Birth, G. S., and G. R. McVey (1968), Measuring the color of growing turf with a reflectance spectrometer, *Agron. J.*, *60*, 640–643.

Bounoua, L., G. J. Collatz, S. O. Los, P. J. Sellers, D. A. Dazlich, C. J. Tucker, and D. A. Randall (2000), Sensitivity of climate to changes in NDVI, *J. Clim.*, *13*, 2277–2292.

Bousquet, P., P. Peylin, P. Ciais, C. Le Quere, P. Friedlingstein, and P. P. Tans (2000), Regional changes in carbon dioxide fluxes of land and oceans since 1980, *Science*, *290*, 1342–1346.

Dickinson, R. E., M. Shaikh, R. Bryant, and L. Graumlich (1998), Interactive canopies for a climate model, *J. Clim.*, *11*, 2823–2836.

Dutton, E. (1994), Aerosol optical depth measurements from four NOAA/CMDL monitoring sites, in *Trends: A Compendium of Data on Global Change*, *ORNL/CDIAC-65*, pp. 484–494, Carbon Dioxide Inf. Anal. Cent., Oak Ridge Natl. Lab., Oak Ridge, Tenn.

Flanagan, L. B., L. A. Wever, and P. J. Carlson (2002), Seasonal and interannual variation in carbon dioxide exchange and carbon balance in a northern temperate grassland, *Global Change Biol.*, *8*, 599–615.

Goward, S. N., C. J. Tucker, and D. G. Dye (1985), North American vegetation patterns observed with the NOAA-7 Advanced Very High Resolution Radiometer, *Vegetatio*, *64*, 3–14.

Goward, S. N., D. G. Dye, S. Turner, and J. Yang (1993), Objective assessment of the NOAA Global Vegetation Index data product, *Int. J. Remote Sens.*, *14*, 3365–3394.

Goward, S. N., S. Turner, D. G. Dye, and S. Liang (1994), The University of Maryland improved Global Land Vegetation Index product, *Int. J. Remote Sens.*, *15*, 3365–3396.

Gutman, G. G. (1991), Vegetation Indices from AVHRR: An update and future prospects, *Remote Sens. Environ.*, *35*, 121–136.

Gutman, G. G. (1999), On the use of long-term global data of land reflectances and vegetation indices derived from the advanced very high resolution radiometer, *J. Geophys. Res.*, *104*(D6), 6241–6255.

Hall, F. G., K. F. Huemmrich, S. J. Goetz, P. J. Sellers, and J. E. Nickeson (1992), Satellite remote-sensing of surface-energy balance: Success, failures, and unresolved issues in FIFE, *J Geophys. Res.*, *97*(D17), 19,061–19,089.

Hansen, J., R. Ruedy, J. Glascoe, and M. Sato (1999), GISS analysis of surface temperature change, *J. Geophys. Res.*, *104*(D24), 30,997–31,022.

Huang, N. E., et al. (1998), The empirical mode decomposition and the Hilbert spectrum for nonlinear and non-stationary time series analysis, *Proc. R. Soc., Ser. A*, *545*, 903–995.

Huang, N. E., et al. (1999), A new view of nonlinear water waves: The Hilbert Spectrum, *Annu. Rev. Fluid Mech.*, *31*, 417–457.

James, M. E., and S. N. V. Kalluri (1994), The Pathfinder land data set: An improved coarse resolution data set for terrestrial monitoring, *Int. J. Remote Sens.*, *15*, 3347–3363.

Ji, L., and A. J. Peters (2003), Assessing vegetation response to drought in the northern Great Plains using vegetation and drought indices, *Remote Sens. Environ.*, *87*, 85–98.

Justice, C. O., J. R. G. Townshend, B. N. Holben, and C. J. Tucker (1985), Analysis of the phenology of global vegetation using meteorological satellite data, *Int. J. Remote Sens.*, *6*, 1271–1381.

Kaminski, T., W. Knorr, P. J. Rayner, and M. Heimann (2002), Assimilating atmospheric data into a terrestrial biosphere model: A case study of the seasonal cycle, *Global Biogeochem. Cycles*, *16*(4), 1066, doi:10.1029/2001GB001463.

Kang, H., Y. Xue, and G. J. Collatz (2006), Impact assessment of satellite-derived leaf area index datasets using a general circulation model, *J. Clim.*, in press.

Langenfelds, R. L., R. J. Francey, B. C. Pak, L. P. Steele, J. Lloyd, C. M. Trudinger, and C. E. Allison (2002), Interannual growth rate variations of atmospheric CO_2 and its delta $\delta^{13}C$, H_2, CH_4, and CO between 1992 and 1999 linked to biomass burning (2002), *Global Biogeochem. Cycles*, *16*(3), 1048, doi:10.1029/2001GB001466.

Los, S. O., C. O. Justice, and C. J. Tucker (1994), A global 1-degrees-by-1-degrees NDVI data set for climate studies derived from the GIMMS Continental NDVI data, *Int. J. Remote Sens.*, *15*, 3493–3518.

Los, S. O., G. J. Collatz, P. J. Sellers, C. M. Malmstrom, N. H. Pollack, R. S. DeFries, L. Bounoua, M. T. Parris, C. J. Tucker, and D. A. Dazlich (2000), A global 9-yr biophysical land surface dataset from NOAA AVHRR data, *J. Hydrometeorol.*, *1*, 183–199.

Los, S. O., P. R. J. North, W. M. F. Grey, and M. J. Barnsley (2005), A method to convert AVHRR Normalized Difference Vegetation Index time series to a standard viewing and illumination geometry, *Remote Sens. Environ.*, *99*, 400–411.

Lucht, W., I. C. Prentice, R. B. Myneni, S. Sitch, P. Friedlingstein, W. Cramer, P. Bousquet, W. Buermann, and B. Smith (2002), Climatic control of the high-latitude vegetation greening trend and Pinatubo effect, *Science*, *296*, 1687–1689.

Masek, J. G., E. F. Vermote, N. Saleous, R. Wolfe, F. G. Hall, F. Huemmrich, F. Gao, J. Kutler, and T. K. Lim (2006), A Landsat surface reflectance data set for North America, 1990–2000, *Geosci. Remote Sens. Lett.*, *3*, 68–72.

Monteith, J. L. (1997), Climate and efficiency of crop production in Britain, *Philos. Trans. R. Soc., Ser. B*, *281*, 271–294.

Myneni, R. B., C. D. Keeling, C. J. Tucker, G. Asrar, and R. R. Nemani (1997), Increased plant growth in the northern high latitudes from 1981–1991, *Nature*, *386*, 698–701.

Nemani, R. R., and S. W. Running (1989), Estimation of resistance to evapotranspiration from NDVI and Thermal-IR AVHRR data, *J. Appl. Meteorol.*, *28*, 276–284.

Nemani, R. R., C. D. Keeling, H. Hashimoto, W. M. Jolly, S. C. Piper, C. J. Tucker, R. B. Myneni, and S. W. Running (2001), Climate-driven increases in global terrestrial net primary production from 1982 to 1999, *Science*, *300*, 1560–1563.

Nemani, R. R., C. D. Keeling, H. Hashimoto, W. M. Jolly, S. C. Piper, C. J. Tucker, R. B. Myneni, and S. W. Running (2003), Climate-driven increases in global terrestrial net primary production from 1982 to 1999, *Science*, *300*, 1560.

Potter, C. S., J. T. Randerson, C. B. Field, P. A. Matson, P. M. Vitousek, H. A. Mooney, and S. A. Klooster (1993), Terrestrial ecosystem production: A process model based on global satellite and surface data, *Global Biogeochem. Cycles*, *7*, 811–841.

Privette, J. L., C. Fowler, G. A. Wick, D. Baldwin, and W. J. Emery (1995), Effects of orbital drift on advanced very high resolution radiometer produces: Normalized difference vegetation index and sea surface temperature, *Remote Sens. Environ.*, *53*, 164–171.

Randerson, J. T., M. V. Thompson, C. M. Malmstrom, C. B. Field, and I. Y. Fung (1996), Substrate limitations for heterotrophs: Implications for models that estimate the seasonal cycle of atmospheric CO_2, *Global Biogeochem. Cycles*, *10*, 585–602.

Rao, C. R. N., and J. Chen (1995), Inter-satellite calibration linkages for the visible and near-infrared channels of the Advanced Very High Resolution Radiometer on the NOAA-u, -9, and -11 spacecraft, *Int. J. Remote Sens.*, *16*, 1931–1942.

Rödenbeck, C., S. Houweling, M. Gloor, and M. Heimann (2003), CO_2 flux history (1982–2001) inferred from atmospheric data using a global inversion of atmospheric transport, *Atmos. Chem. Phys.*, *3*, 1919–1964.

Rosen, J. M., et al. (1994), Decay of Mount Pinatubo aerosol at midlatitudes in the Northern and Southern Hemispheres, *J. Geophys. Res.*, *99*(D12), 25,733–25,739.

Rouse, J. W., R. H. Haas, J. A. Schell, D. W. Deering, and J. C. Harlan (1974), Monitoring the vernal advancement and retrogradation (greenwave effect) of natural vegetation, *Rep. RSC 1978-4*, Remote Sens. Cent., Texas A&M Univ., College Station, Tex.

Russell, P. B., et al. (1993), Pinatubo and pre-Pinatubo optical-depth spectra: Mauna Loa measurements, comparisons, inferred particle size distributions, radiative effects, and relationships to lidar data, *J. Geophys. Res.*, *98*(D12), 22,969–22,985.

Sato, M., et al. (1993), Stratospheric aerosol optical depths, 1850–1990, *J. Geophys. Res.*, *98*(D12), 22,987–22,994.

Schimel, D., and D. Baker (2002), Carbon cycle: The wildfire factor, *Nature*, *420*, 29–30.

Sellers, P. J. (1985), Canopy reflectance, photosynthesis, and transpiration, *Int. J. Remote Sens.*, *6*, 1335–1371.

Sellers, P. J., D. A. Randall, C. J. Collatz, J. A. Berry, C. B. Field, D. A. Dazlich, C. Zhang, C. D. Collelo, and L. Bounoua (1996), A revised land surface parameterization (SiB2) for atmospheric GCMs: Part 1. Model formulation, *J. Clim.*, *9*, 676–705.

Tian, H., J. M. Melillo, D. W. Kicklighter, A. D. McGuire, J. V. K. Helfrich, B. Moore, and C. J. Vörösmarty (1998), Effect of interannual climate variability on carbon storage in Amazonian ecosystems, *Nature*, *396*, 664–667.

Townshend, J. R. G. (1994), Global data sets for land applications from the Advanced Very High Resolution Radiometer: An introduction, *Int. J. Remote Sens.*, *15*, 3319–3332.

Tucker, C. J. (1979), Red and photographic infrared linear combination for monitoring vegetation, *Remote Sens. Environ.*, *8*, 127–150.

Tucker, C. J., J. R. G. Townshend, and T. E. Goff (1985), African land-cover classification using satellite data, *Science*, *227*, 369–375.

Tucker, C. J., Y. Fung, C. D. Keeling, and R. H. Gammon (1986), Relationship between atmospheric CO_2 variations and a satellite-derived vegetation index, *Nature*, *319*, 195–199.

Tucker, C. J., W. W. Newcomb, and H. E. Dregne (1994), AVHRR datasets for the determination of desert spatial extent, *Int. J. Remote Sens.*, *15*, 3547–3566.

Tucker, C. J., J. E. Pinzon, M. E. Brown, D. A. Slayback, E. W. Pak, R. Mahoney, E. F. Vermote, and N. El Saleous (2005), An extended AVHRR 8-km NDVI dataset compatible with MODIS and SPOT vegetation NDVI data, *Int. J. Remote Sens.*, *26*, 4485–4498.

van der Werf, G. R., J. T. Randerson, G. J. Collatz, L. Giglio, P. S. Kasibhatla, A. F. Arellano, S. C. Olsen, and E. S. Kasischke (2004), Continental-scale partitioning of fire emissions during the 1997 to 2001 El Nino/La Nina period, *Science*, *303*, 73–76.

Vermote, E., and Y. J. Kaufman (1995), Absolute calibration of AVHRR visible and near-infrared channels using ocean and cloud views, *Int. J. Remote Sens.*, *16*, 2317–2340.

Vermote, E., et al. (1997), Data pre-processing: Stratospheric aerosol perturbing effect on the remote sensing of vegetation: Correction method for the composite NDVI after the Pinatubo eruption, *Remote Sens. Rev.*, *15*, 7–21.

Wanner, W., X. Li, and A. H. Strahler (1995), On the derivation of kernels for kernel-driven models of bidirectional reflectance, *J. Geophys. Res.*, *100*(D10), 21,077–21,089.

Zeng, N., J. D. Neelin, K. M. Lau, and C. J. Tucker (1999), Enhancement of interdecadal climate variability in the Sahel by vegetation interaction, *Science*, *286*, 1537–1540.

Zeng, N., A. Mariotti, and P. Wetzel (2005), Terrestrial mechanisms of interannual CO_2 variability, *Global Biogeochem. Cycles*, *19*, GB1016, doi:10.1029/2004GB002273.

Zhang, Y.-C., W. B. Rossow, A. A. Lacis, V. Oinas, and M. I. Mishchenko (2004), Calculation of radiative fluxes from the surface to top of atmosphere based on ISCCP and other global data sets: Refinements of the radiative transfer model and the input data, *J. Geophys. Res.*, *109*, D19105, doi:10.1029/2003JD004457.

Zhou, L., R. K. Kaufmann, Y. Tian, R. B. Myneni, and C. J. Tucker (2003), Relation between interannual variations in satellite measures of vegetation greenness and climate between 1982 and 1999, *J. Geophys. Res.*, *108*(D1), 4004, doi:10.1029/2002JD002510.

G. J. Collatz, F. Hall, and J. G. Masek, NASA Goddard Space Flight Center, Code 614.4, Greenbelt, MD 20771, USA. (fghall@ltpmail.gsfc.nasa.gov)